RSC Advances

ROYAL SOCIETY OF CHEMISTRY

www.rsc.org/advances

4-Oxo- or 1-Oxo-N_7O^+? A Computational and Experimental Study †

Tao Yu,[*a,c] Ying-Zhe Liu,[a] Ralf Haiges,[b] Karl O. Christe,[*b] Wei-Peng Lai[a] and Bo Wu[*c]

Received (in XXX, XXX) Xth XXXXXXXXX 200X, Accepted Xth XXXXXXXXX 200X
DOI: 10.1039/b000000x

In a previous paper [*Inorg. Chem.*, 2010, **49**, 1245], we studied the reaction of F_2NO^+ with an excess of HN_3 which led to the quantitative formation of N_5^+ and N_2O. Based on ^{15}N-labeling experiments and theoretical calculations, the formation of a 4-oxo-N_7O^+ intermediate with a decomposition energy barrier of about 40 kcal/mol was proposed. Since this relatively high barrier disagreed with our failure to experimentally observe this cation, a thorough theoretical study of the isomerization, dissociation and formation pathways of N_4FO^+ and N_7O^+ was carried out at the B3LYP and G3B3 levels at 240 K. It was found that the self-decomposition of 4-oxo-N_7O^+ to NO^+ and N_2 has a considerably lower barrier of only 19.6 kcal/mol and, therefore, would be more likely than a self-decomposition to N_5^+ and N_2O. Additional calculations also showed that alternate reaction pathways between the stable and well-characterized *z*-N_4FO^+ intermediate product and HN_3 involving 7- or 9-membered cyclic transition states, can lead to the observed N_5^+ and N_2O products with the observed ^{15}N distribution and barriers as low as 20.7 kcal/mol. The transition states for these reactions contain a 1-oxo-N_7O^+ component which can decompose without a barrier to N_5^+ and N_2O. These alternate pathways involving an unstable 1-oxo-N_7O^+ cation are in better agreement with experiment than the one involving 4-oxo-N_7O^+. The correctness of this re-interpretation was experimentally verified by a ^{15}N-labeling experiment between α- and γ- ^{15}N-labeled HN_3 and unlabeled N_4FO^+ which resulted exclusively in unlabeled N_2O and α- and γ- ^{15}N-labeled N_5^+. Therefore, we conclude that in the reaction of NF_2O^+ with excess HN_3 the experimental and theoretical evidence supports only the formation of an unstable 1-oxo-N_7O^+ cation, and that for the preparation of the symmetric 4-oxo-N_7O^+ cation different synthetic approaches will be required.

Introduction

Polynitrogen compounds are of great interest as energetic materials.[1-3] In 1999, N_5^+ was synthesized by the reaction of HN_3 with N_2F^+ at -78 °C in dry HF (Scheme 1).[2]

$$N_2F^+ + HN_3 \rightarrow N_5^+ + HF$$

Scheme 1 Synthesis of the N_5^+ cation.

Application of the same approach to the reaction of the closely related NF_2O^+ cation with HN_3 resulted in the formation of the stable *z*-N_4FO^+ and *e*-N_4FO^+ cations, when a 1:1 mole ratio of the starting materials was used (Scheme 2).[3]

$$NF_2O^+ + HN_3 \rightarrow N_4FO^+ + HF$$

Scheme 2 Synthesis of the N_4FO^+ cations.

However, when an excess of HN_3 was used, the expected N_7O^+ cation (Scheme 3) could not be experimentally observed even at low temperatures.[4]

$$NF_2O^+ + 2\,HN_3 \rightarrow N_7O^+ + 2\,HF$$

Scheme 3 Attempted synthesis of N_7O^+.

Surprisingly, N_5^+ and N_2O were observed in quantitative yield as the only reaction products (Scheme 4).

$$NF_2O^+ + 2\,HN_3 \rightarrow N_5^+ + N_2O + 2\,HF$$

Scheme 4 Observed reaction products from the reaction of NF_2O^+ with 2 moles of HN_3.

Based on theoretical calculations and a ^{15}N-labeling experiment, using unlabeled NF_2O^+ and α- and γ- ^{15}N-labeled HN_3, which resulted in terminally labeled N_2O and N_5^+ labeled equally in all five positions, the formation of a 4-oxo-N_7O^+ intermediate was proposed.[4] However, this interpretation presented a major problem. The predicted barrier for the decomposition of 4-oxo-N_7O^+ to N_5^+ and N_2O had a high value of ~42 kcal/mol.[4] This high barrier should have allowed its experimental observation. This discrepancy prompted the Chinese group to carry out a very intensive computational study which suggested a more likely alternate reaction path with a much lower activation energy barrier of only 20.7 kcal/mol, while also replicating the observed ^{15}N-labeled products. The correctness of the alternate reaction scheme was experimentally verified by the American group by a second ^{15}N-labeling experiment. The detailed results of these combined studies are presented in this paper, showing that 1-oxo-N_7O^+ is much less stable to decomposition to N_5^+ and N_2O than the 4-oxo isomer and is the likely unobserved unstable intermediate in the reaction of NF_2O^+ with an excess of HN_3.

Results and discussion

A. Selection of computational method

In this section, we first test the applicability of the B3LYP, MP2 and CCSD(T) methods by comparing the optimized structures of small molecules and cations (**1** to **6**) which are related to the reaction of N_7O^+, with corresponding known experimental structures,[5-9] and by calculating their enthalpies of formation. The most important structural parameters of **1** to **6** optimized with the B3LYP, MP2 and CCSD(T) methods, are shown in Fig. 1.

Compared with the experimental values, the B3LYP method slightly overestimates bond lengths of **1** to **6**, but the deviations are within 0.01 Å (except for the N-O bond in **1**), while the deviations of the bond angles are within 2°. Thus, the B3LYP method can provide satisfactory geometries for the systems of interest. The CCSD(T) method performs excellently when compared to the experimental geometries in gas phase. The deviations of bond lengths of **2**, **3**, **4** and **6** are less than 0.004 Å, and 0.2° on bond angles of **2**. However, the CCSD(T)/aug-cc-pVQZ calculations are costly. The performance of MP2 is not as good as expected, especially for the short N-N bonds in **2**, **4**, **5** and **6**.

The computed enthalpies of formation of **1** to **6** using the B3LYP, MP2, CCSD(T) and G3B3 methods and experimental enthalpies of formation of **1** to **4** and **6** are presented in Table 1. Among the four computational methods, the computed values of the composite G3B3 method for **1** to **4** and **6** are the closest to experiment, and the deviations are within 1 kcal/mol. The deviation between G3B3 and CCSD(T) of complete basis set (353.3 kcal/mol was predicted by the best available calculation[10]) is about 2 kcal/mol. Compared with experimental (**1** to **4**) or G3B3 (**5** and **6**) values, the absolute deviations of B3LYP, MP2 and CCSD(T) are 1.2 to 3.4, 4.2 to 26.4 and 0.4 to 10.7 kcal/mol, respectively. Evidently, the G3B3 method can evaluate precise energies, and the B3LYP calculations achieve acceptable accuracy at moderate cost. MP2 fails to predict the precise enthalpies of formation for polynitrogen system and provides a negative enthalpy of formation for **4**. The results of Pople's 6-311++G** and Petersson's CBS-QB3 are also presented in Fig. S1 and Table S1 of ESI. There are little difference between B3LYP/aug-cc-pVDZ and B3LYP/6-311++G** geometries. The enthalpies of formation of B3LYP/aug-cc-pVDZ and G3B3 are a little better than those of B3LYP/6-311++G** and CBS-QB3, respectively.

On the basis of the above results, we will use in the following discussions B3LYP to optimize all of the geometries, and B3LYP and G3B3 to explore the reaction pathways and to calculate the free energy activation barriers. Unless otherwise specified, G3B3 energies are mainly used in the text. Numbering schemes for the compounds and cations are given in Fig. S2 of the ESI. The notations for the transition states and complexes are **TS** and **C**, respectively, followed by the numbers of compounds and cations.

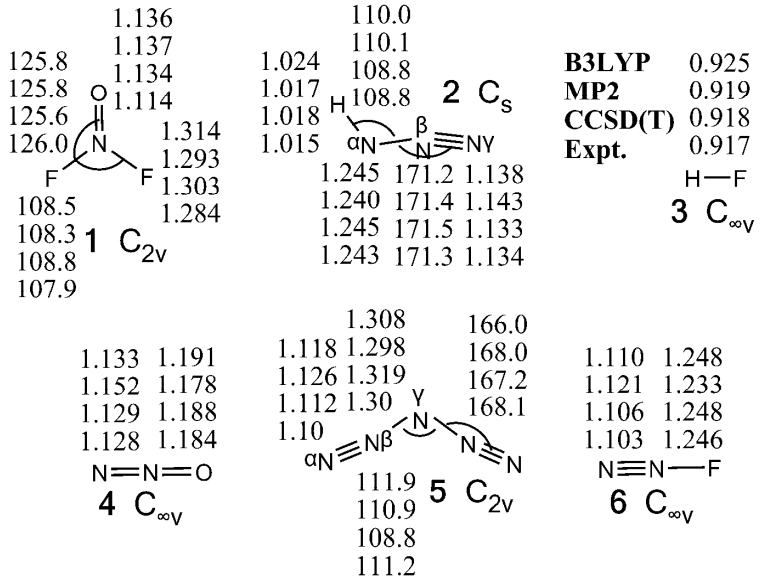

Fig. 1 Computed (at B3LYP/aug-cc-pVDZ, MP2/aug-cc-pVQZ, and CCSD(T)/aug-cc-pVQZ levels) and experimental geometries of F_2NO^+ (**1**), HN_3 (**2**), HF (**3**), N_2O (**4**), N_5^+ (**5**) and N_2F^+ (**6**). The bond lengths in angstroms and bond angles in degrees. The experimental geometries: F_2NO^+,[5] crystal structure of $F_2NO^+AsF_6^-$; HN_3,[6] microwave spectroscopy; HF,[7] microwave spectroscopy; N_2O,[7] infrared and Raman spectroscopy; N_5^+,[8] crystal structure of $N_5^+Sb_2F_{11}^-$; and N_2F^+,[9] millimeter-wave spectroscopy.

Table 1 Computed[α] (at B3LYP/aug-cc-pVDZ, MP2/aug-cc-pVQZ, CCSD(T)/aug-cc-pVQZ, and G3B3 levels) and experimental[β] enthalpies (in kcal/mol) of formation in the gas phase at 298.15 K for $NF2O^+$, HN_3, HF, N_2O, N_5^+ and N_2F^+.

Species	B3LYP	MP2	CCSD(T)	G3B3	Expt.
NF_2O^+ (**1**)	234.6	212.8	237.6	233.4	232.4
HN_3 (**2**)	68.0	56.9	77.3	70.0	70.3
HF (**3**)	-61.8	-69.4	-64.8	-65.2	-65.1
N_2O (**4**)	21.7	-0.6	26.3	19.4	19.6
N_5^+ (**5**)	348.4	324.8	361.9	351.2	-
N_2F^+ (**6**)	293.5	274.8	295.5	290.6	283.4±4.6

[α]The enthalpies of formation were calculated from the atomic energies in the gas phase. The ionization energy of the nitrogen atom was used to calculate the enthalpies of formation of the cations.

[β]The experimental enthalpies of formation, the atomic energies, the ionization energy of the nitrogen atom, and the appearance energies of NF_3O and *cis*-N_2F_2 are taken from ref. 7.

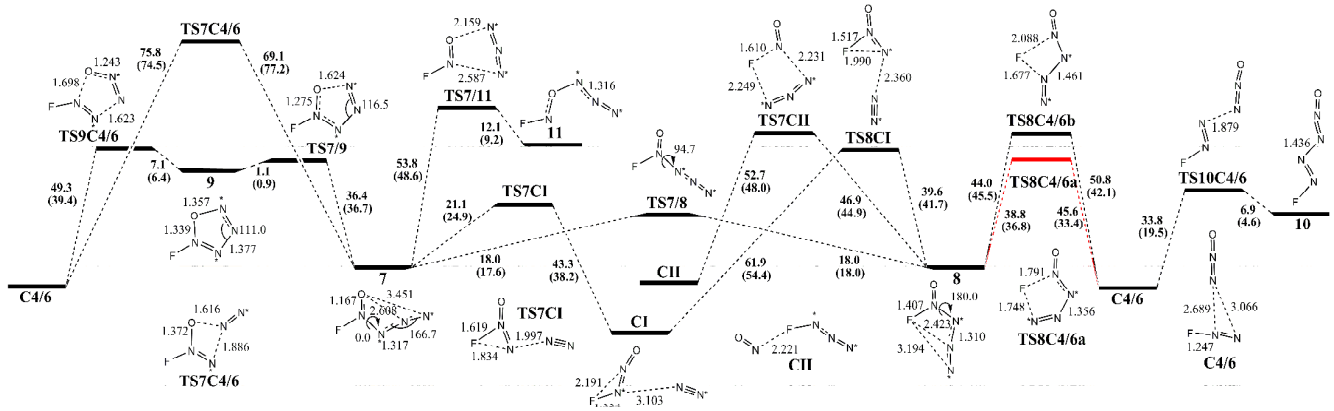

Fig. 2 Schematic potential energy surface around N_4OF^+ at the G3B3 level. The activation free energy barriers at 240 K in kcal/mol, (B3LYP/aug-cc-pVDZ values in parentheses), bond lengths in angstroms, and bond and dihedral angles in degrees. The possible nitrogen atoms labeled by ^{15}N with asterisks, the pathway which agrees with the observed ^{15}N labels is shown in red, and all the systems are with one positive charge.

B. Isomerization and dissociation of N_4OF^+

In this investigation, five isomers (**7** to **11**) of N_4FO^+ were optimized. The isomerization and dissociation pathways of these isomers are shown in Fig. 2. The isomers with the two lowest free energies are **7** (*e*) and **8** (*z*), and their free energies are almost the same. The isomerization barrier from **7** to **8** is 18.0 kcal/mol, and the reverse barrier is equal to the forward one. Consequently, there is no thermodynamically dominant geometry for **7** and **8**. The dissociation of **9** to **C4/6**, the ring opening of **9** to **7**, dissociation of **10** to **C4/6,** and transformation of **11** to **7** cross barriers of less than 15 kcal/mol, which implies that **9**, **10** and **11** dissociate or transform easily. **11** can also decompose to NF, NO^+ and N_2 with a 3.1 kcal/mol barrier (see Fig. S3). Hence, **7** and **8** are the two primary isomers of N_4FO^+.

The dissociation of **7** to **C4/6** has two pathways: one is concerted, and the other one is a stepwise pathway via the intermediate **9**. The concerted pathway via **TS7C4/6** has a very high barrier of 69.1 kcal/mol. Because the dissociation barrier of **9** to **C4/6**, i.e., the second step of the dissociation of **7** to **C4/6**, is only 7.1 kcal/mol, the limiting step is the first step, i.e., the cyclization of **7** to **9** via **TS7/9** with a high barrier of 36.4 kcal/mol. The dissociation of **8** to **C4/6** also has two pathways: F can approach either *β*-N (**TS8C4/6b**) or *γ*-N (**TS8C4/6a**). The dissociation barrier for **8** to **C4/6** via **TS8C4/6a** is 38.8 kcal/mol, and via **TS8C4/6b** it is 44.0 kcal/mol. Therefore the dissociation of *z*- and *e*-N_4FO^+ to N_2F^+ and N_2O will not proceed easily.

Furthermore, decomposition of N_4FO^+ to N_2F^+ and N_2O is not supported by the experimentally observed decomposition of *α*- and *γ*-^{15}N-labeled N_4FO^+ to unlabeled NO^+, labeled N_2 and NF_3 (Scheme 5).

$$3\ N_4FO^+ \rightarrow 3\ NO^+ + 4\ N_2 + NF_3$$

Scheme 5 Experimentally observed decomposition of N_4FO^+.

However, we found the following more likely pathway. The *e*-N_4FO^+ cation (**7**) can go through the transition state (**TS7CI**) involving the breakage of the *α*-N-*β*-N bond and an F shift from N(O) to *α*-N, with a dissociation barrier of only 21.1 kcal/mol. The *z*-N_4FO^+ cation (**8**) has a similar pathway via **TS8CI**, but the barrier is somewhat higher (39.6 kcal/mol). $ONNF^+$ in **CI** can decompose to NO^+ and N_2 with a 27.2 kcal/mol barrier (see Fig. S4). The barrier from **8** to NO^+ and FN_3 (**CII**) is 46.9 kcal/mol and is considerably larger. Therefore, the most favorable decomposition pathways of **7** and **8** are **7→TS7CI→CI** and **8→TS7/8→7→TS7CI→CI**, respectively, with maximum barriers of 21.1 kcal/mol.

Due to a potential catalysis by HF (**3**), the dissociation of *z*-N_4FO^+ (**8**) in the presence of **3** was also studied. However, as shown in Fig. S5, the participation of HF increases the dissociation barriers to more than 60 kcal/mol. Thus, these pathways can be ruled out.

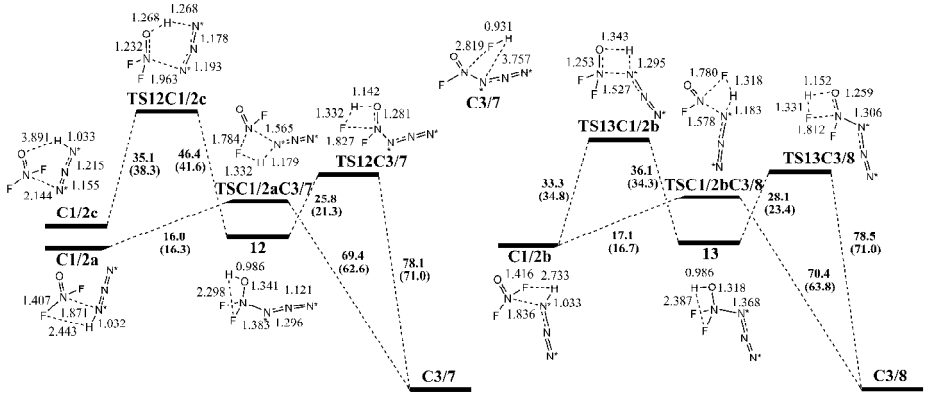

Fig. 3 Schematic potential energy surfaces around $F_2NO^+ + HN_3$ at the G3B3 level. The activation free energy barriers at 240 K in kcal/mol, (B3LYP/aug-cc-pVDZ values in parentheses), and bond lengths in angstroms. The possible nitrogen atoms labeled by ^{15}N are marked with asterisks, and all the systems possess one positive charge.

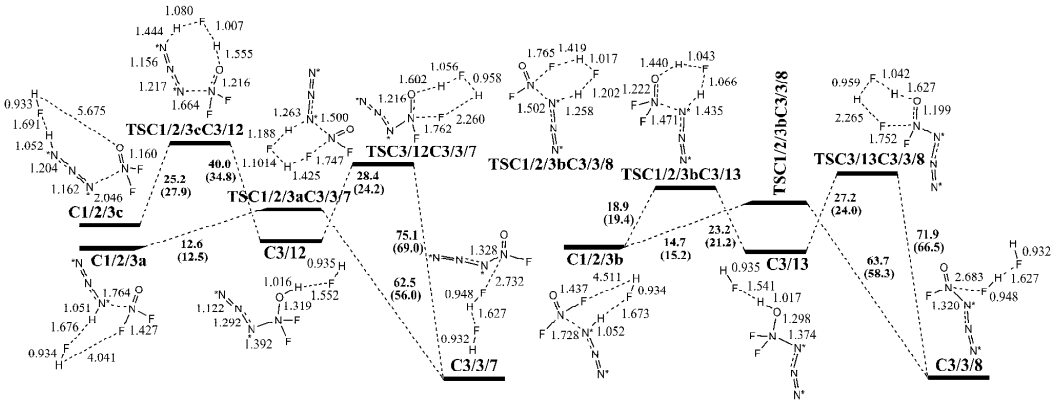

Fig. 4 Schematic potential energy surfaces around $F_2NO^+ + HN_3 + HF$ at the G3B3 level. The activation free energy barriers at 240 K in kcal/mol, (B3LYP/aug-cc-pVDZ values in parentheses), and bond lengths in angstroms. The possible nitrogen atoms labeled by ^{15}N are marked with asterisks, and all the systems possess one positive charge.

C. Formation of N_4OF^+

The reactions of NF_2O^+ (**1**) with HN_3 (**2**) in the absence of HF leading to the formation of *e*-N_4FO^+ (**7**) and *z*-N_4FO^+ (**8**) are shown in Fig. 3. During the reaction of **1** with **2**, the different interactions between two molecules can involve three complexes (**C1/2a**, **C1/2b** and **C1/2c**) as reaction entrances, among which **C1/2a** ultimately forms **C3/7** along a concerted pathway with a barrier of 16.0 kcal/mol, and **C1/2c** ultimately forms **C3/7** along a stepwise pathway with one intermediate and two transition states with a maximum barrier of 35.1 kcal/mol, while **C1/2b** ultimately forms **C3/8** along either a concerted pathway with a barrier of 17.1 kcal/mol or a stepwise pathway with one intermediate and two transition states with a maximum barrier of 33.3 kcal/mol. Obviously, from a thermodynamic point of view, the preferred formation pathways of **7** and **8** are the concerted ones from **C1/2a** and **C1/2b**, respectively. It should be noted that in the transition states along the concerted pathways the hydrogen atom is still bound to nitrogen and bridges to an F atom, while in the first step of the stepwise pathways, the H atom attaches itself to the O atom and starts to depart from the α-N atom, resulting in a higher barrier.

Since the reaction of NF_2O^+ with HN_3 was carried out in HF solution, it was important to study the reactions of **1** with **2** in the presence of HF (Fig. 4). As can be seen, HF significantly lowers the barriers for the formation of **7** and **8**, and catalyzes the reaction of **1** with **2**. Since HF is one of the reaction products, this reaction is auto-catalytic, similar to our previous report on the auto-catalysis of polyesterification.[11] However, the presence of HF does not change the barrier ordering of these pathways, and the preferred formation pathways of **7** and **8** are still the concerted ones from **C1/2/3a** and **C1/2/3b**, respectively. The corresponding barriers are 12.6 and 14.7 kcal/mol, respectively.

Comparing the barriers of the concerted reaction pathways via **C1/2a** and **C1/2b**, it is found that, independent of the absence or presence of HF, the barriers for the formation of **7** and **8** are always very similar, and no low-barrier pathways for the formation of **9**, **10** and **11** from **1** and **2** as reactants were discovered. Therefore the reaction of **1** with **2** produces both **7** and **8**.

D. Formation of N_5^+ via N_2F^+ and HN_3

The direct formation mechanism of N_5^+ (**5**) from N_2F^+ (**6**) and HN_3 (**2**) has been reported.[12] Our calculations indicated that the barrier from **C2/6** to **C3/5** is 10.2 kcal/mol (Fig. 6). We have also investigated the reaction of **2** with **6** in the presence of HF (**3**). It was found that a transition state with a six-membered ring is formed (**TSC2/3/6C3/3/5** in Fig. 6) along the pathway, and the corresponding barrier is only 6.6 kcal/mol. Hence, this is the preferred pathway to the formation of **5** from **2** and **6**, and HF takes part in the reaction as a catalyst. The formation of **5** via **2** and **6** is not the limiting pathway.

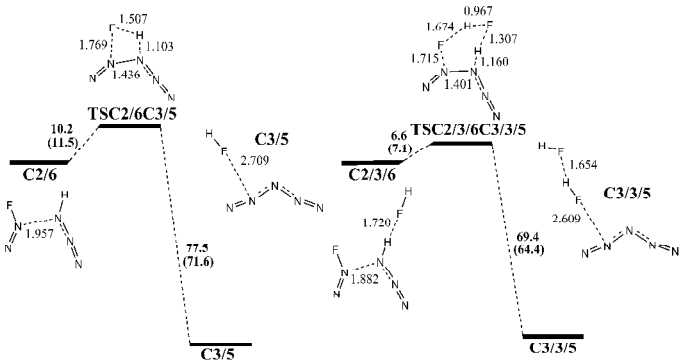

Fig. 5 Schematic potential energy surfaces of formation of N_5^+ at the G3B3 level. The activation free energy barriers at 240 K in kcal/mol, (B3LYP/aug-cc-pVDZ values in parentheses), bond lengths in angstroms, and all the systems possess one positive charge.

E. Isomerization and self-dissociation of N_7O^+

In our calculations, six isomers (**14** to **19**) of N_7O^+ were found. Their isomerization and dissociation pathways are shown in Fig. 6. The **14**, **15** and **16** isomers are the three possible 4-oxo-isomers, i.e., the oxygen is attached to the central nitrogen atom, and the two azido ligands point either in the same direction as the oxygen (**15**) (*syn-syn*), in the opposite direction (**16**) (*anti-anti*), or one in the same direction and the other one in the opposite direction (**14**) (*syn-anti*). The (*anti-anti*) isomer **16** lies 14.6 kcal/mol above the (*syn-anti*) isomer **14** and its isomerization barrier to **14** is only 1.0 kcal/mol. Hence **16** is highly unstable and was not further considered. The (*syn-syn*) isomer **15** is the lowest in energy and lies 1.9 kcal/mol below the (*syn-anti*) isomer **14**. The isomerization barrier for the conversion of (*anti-syn*) **14** to (*syn-syn*) **15** is also low and amounts only to 11.3 kcal/mol. Isomers **17** and **18** are cyclic isomers and lie 24.2 and 23.0

kcal/mol,

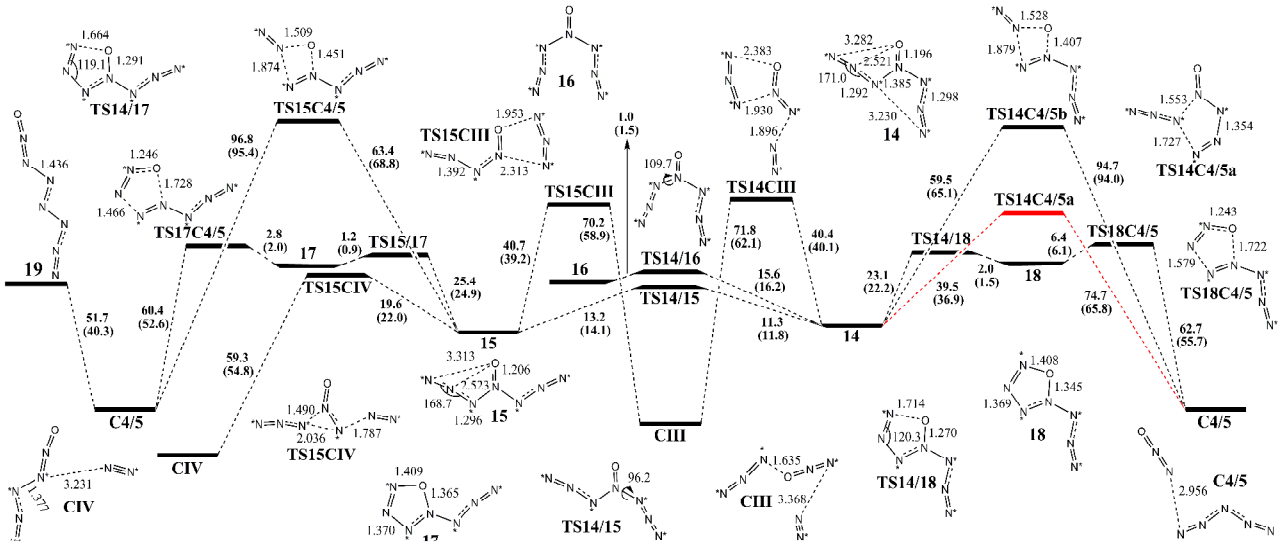

Fig. 6 Schematic potential energy surfaces around N_7O^+ at the G3B3 level. The activation free energy barriers at 240 K in kcal/mol, (B3LYP/aug-cc-pVDZ values in parentheses), bond lengths in angstroms, and bond and dihedral angles in degrees. The possible nitrogen atoms labeled by ^{15}N are marked with asterisks, the pathway in conformity with the ^{15}N labels is shown in red, and all the systems are with one positive charge.

respectively, above the (*syn-syn*) isomer **15**. Compound **19** is the 1-oxo-isomer and lies 18.3 kcal/mol above **15**. Thus, (*syn-syn*) **15** is the dominant isomer of N_7O^+.

The dissociation of (*anti-syn*) N_7O^+ **14** to N_2O (**4**) and N_5^+ (**5**) can proceed along three different pathways: 1) the formation of a new N-N bond between the α and γ positions via **TS14C4/5a** with a five-membered ring and a barrier of 39.5 kcal/mol; 2) a dissociation pathway involving the **TS14C4/5b** transition state with a four-membered ring and a high barrier of 59.5 kcal/mol; 3) a stepwise pathway involving an intermediate (**18**) with a five-membered ring crossing a lower barrier of 23.1 kcal/mol. Similarly, the dissociation of (*syn-syn*) N_7O^+ **15** to N_2O (**4**) and N_5^+ (**5**) can proceed along two different pathways: 1) a dissociation pathway involving only one transition state with a four-membered ring, **TS15C4/5**, with a very high barrier of 63.4 kcal/mol; 2) a stepwise pathway involving an intermediate (**17**) with a five-membered ring crossing a lower barrier of 25.4 kcal/mol. These conclusions are consistent with those from the previous investigation.[4] Based on these barriers and whether starting from **14** or **15**, the most favorable dissociations are the stepwise pathways with ring-like intermediates. These intermediates, **17** and **18**, are isomers of N_7O^+. They are located in a shallow potential well and their isomerization or dissociation barriers are only several kcal/mol. However, they tend to isomerize rather than dissociate because the barriers of isomerization are lower than those of dissociation by about 1 kcal/mol. Although from a thermodynamic point of view these stepwise pathways having barriers as low as 23.1 kcal/mol might be worthy of consideration, they must be rejected because they do not result in the experimentally observed ^{15}N labels.

Another important result from our calculations is the finding that the barrier for the conversion of the 1-oxo-N_7O^+ isomer **19** to N_2O **4** and N_5^+ **5** (not denoted in Fig. 6) is only 0.2 kcal/mol (0 K without zero-point vibrational energy) at the B3LYP level. Therefore, **19** is able to dissociate very easily into **4** and **5**, while reproducing the previously reported ^{15}N labels. Although **19** cannot be directly prepared from NF_2O^+ and excess HN_3, it is present as a component of the important **TSC2/3/8C3/3/4/5a** transition state in the reaction of N_4FO^+ with HN_3 in the presence of HF and thus provides the best explanation for all of our experimental observations, including the additional ^{15}N-labeling experiments which will be described below.

There are also three possible pathways for the decomposition of N_7O^+ to N_3^+ or NO^+: 1) (*anti-syn*) N_7O^+ **14** decomposes to N_3^+ with evolution of N_2 and NO_2 via **TS14CIII**. It undergoes the break of the α-N-β-N bond on one side and the break of the α-N-N(O) bond on the other side with a barrier of 40.4 kcal/mol; 2) (*syn-syn*) N_7O^+ **15** decomposes to N_3^+ via **TS14CIII** with a barrier of 40.7 kcal/mol; 3) the pathway of dissociation to N_5O^+ goes through a transition state (**TS15CIV**) involving the break of a α-N-β-N bond and an azide group shifts from N(O) to α-N with a dissociation barrier of 19.6 kcal/mol. N_5O^+ in **CIV** readily decomposes to NO^+ with evolution of N_2 with a barrier of only 5.8 kcal/mol (Fig. S6). Therefore, the optimum pathways of decomposition of **14** and **15** are **14→TS14/15→15→TS15CIV→CIV** and **15→TS15CIV→CIV**, respectively. Again, the barrier of 19.6 kcal/mol would be reasonably low, but these pathways cannot explain the experimentally observed reaction of NF_2O^+ with excess HN_3 which produced equally labeled N_5^+ and terminally labeled N_2O.[4]

F. Dissociation of N_7O^+ with excess HN_3

Due to the presence of excess HN_3 in the reaction system, the dissociation of N_7O^+ in the presence of HN_3 was also investigated. The corresponding dissociation pathways are displayed in Fig. 7. The presence of HN_3 lowers the dissociation barrier of **14** to **C4/5** along the concerted pathway, with the H atom attaching to the α-N of **14** and departing from the α-N of HN_3, but the barrier of 44.9 kcal/mol is still high. The barrier order parallels again the electronegativity order. At the same time, in the presence of HN_3, the *anti*/*syn* isomerization of N_7O^+

was found via an intermediate **C5/20**, but for both isomerization directions, from **14** to **15** or from **15** to **14**, the barriers are more than 30 kcal/mol. Thus the presence of HN_3 does not facilitate the isomerization, compared to the reaction in its absence (see Fig. 6). It should be mentioned that the processes give rise to the formation of N_5^+. In addition, the dissociation of N_5OH^+ **20** was investigated. It undergoes two transition states with one intermediate in between (Fig. S7). Both barriers are not more than 8 kcal/mol and are lower than the barriers of the reaction of **20** with **5** back to **14** and **15**. Thus, the intermediate **20** rather dissociates than transforms to **14** or **15**, and the dissociation barriers of **14** and **15** with excess HN_3 are 30.6 and 32.5 kcal/mol, respectively.

The stepwise N_7O^+ decomposition mechanisms involve attachment of the azide groups to N(O) in the first step and decomposition through **TS14C4/5a** (Fig. 6) in the second step. The intermediates **22** and **23** (Fig. 7) are novel with ten nitrogen atoms. The performance of these stepwise pathways is still poor, because they cross limiting barriers of more than 50 kcal/mol.

Because of the catalytic effect of HF, the dissociation of N_7O^+ in the presence of HN_3 and HF was also studied. The corresponding dissociation pathways are presented in Fig. 8. There is no significant change in the presence of HF, compared to the presence of HN_3 only. The lowest dissociation barriers of **14** and **15** with excess HN_3 in the presence of HF are 33.6 and 33.4 kcal/mol, respectively.

All the pathways in Figs. 7 and 8 are in accord with the experimental ^{15}N labels.[4] Moreover, we tried to calculate the barriers of reactions between **15** and HF. However, barriers in excess of 60 kcal/mol must be overcome. In summary, the barriers of dissociation of **14** and **15** in the presence of HN_3 are higher than 30 kcal/mol, and the reactions are not catalyzed.

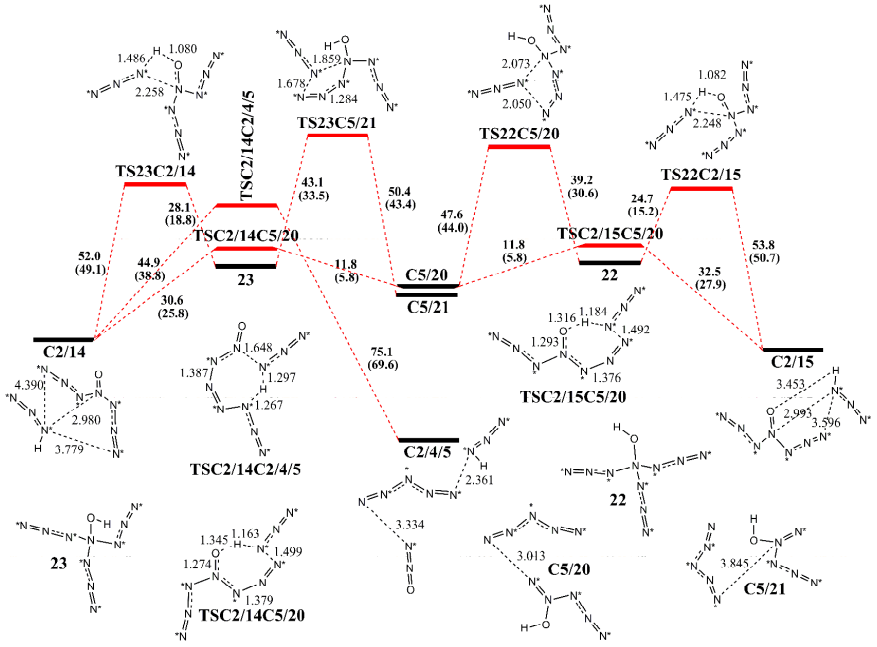

Fig. 7 Schematic potential energy surface around $N7O^+$ + HN3 at the G3B3 level. The activation free energy barriers at 240 K in kcal/mol, (B3LYP/aug-cc-pVDZ values in parentheses), and bond lengths in angstroms. The possible nitrogen atoms labeled by ^{15}N are marked with asterisks, the pathways in conformity with the ^{15}N labels are shown in red, and all the systems are with one positive charge.

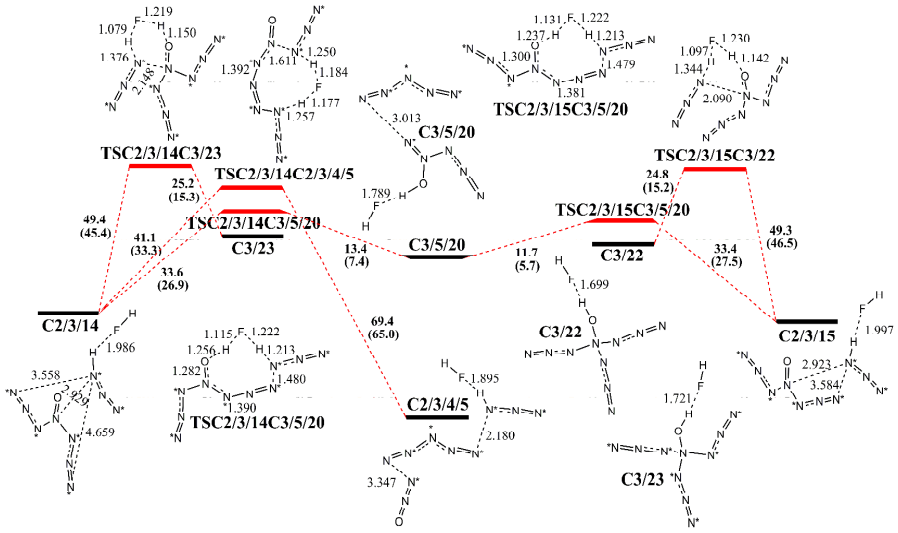

Fig. 8 Schematic potential energy surfaces around N_7O^+ + HN_3 + HF at the G3B3 level. The activation free energy barriers at 240 K in kcal/mol,

(B3LYP/aug-cc-pVDZ values in parentheses), and bond lengths in angstroms. The possible nitrogen atoms labeled by ^{15}N are marked with asterisks, the pathways in conformity with the ^{15}N labels are shown in red, and all the systems are with one positive charge.

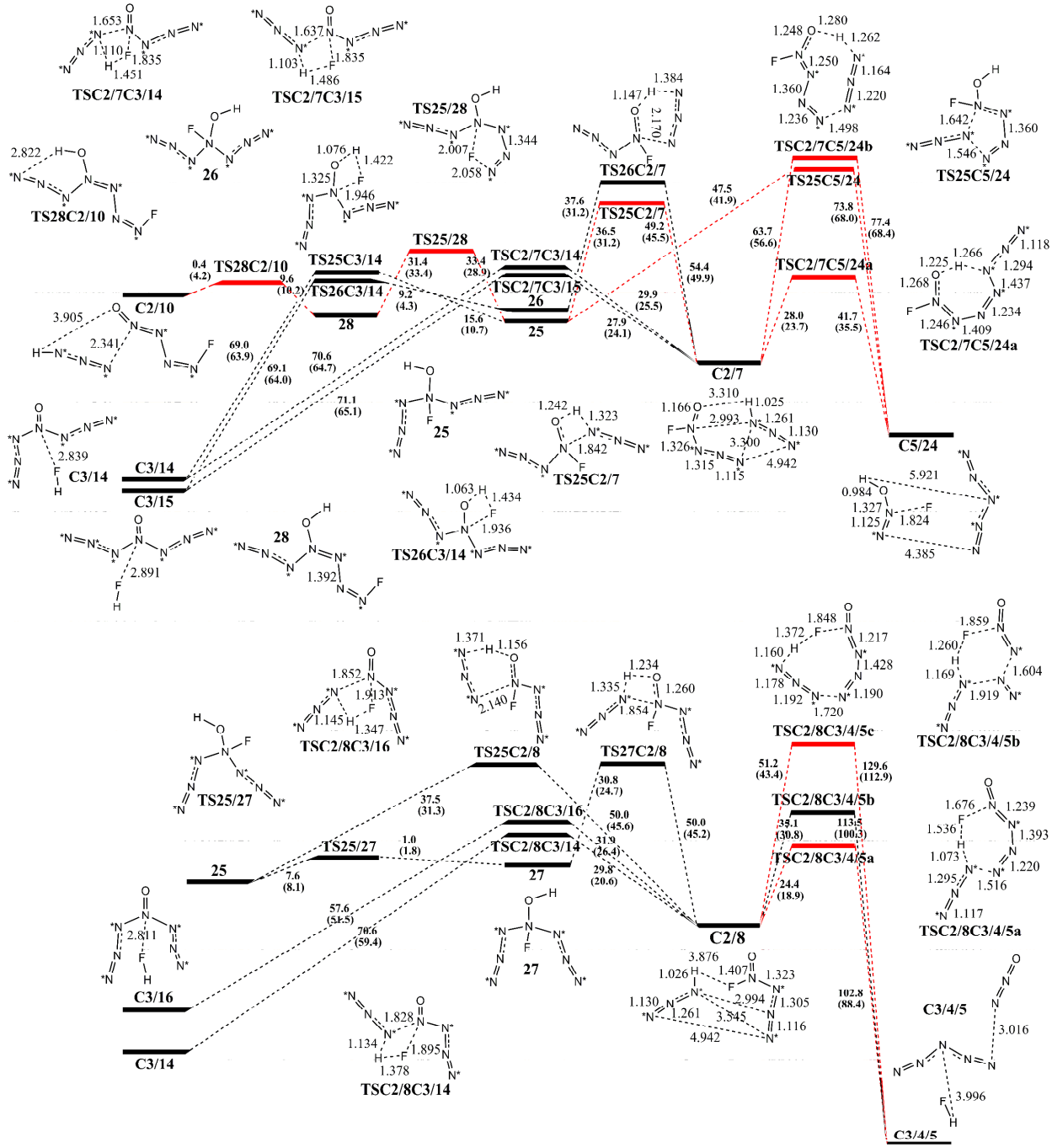

Fig. 9 Schematic potential energy surfaces around $N_4OF^+ + HN_3$ at the G3B3 level. The activation free energy barriers at 240 K in kcal/mol, (B3LYP/aug-cc-pVDZ values in parentheses), and bond lengths in angstroms. The possible nitrogen atoms labeled by ^{15}N are marked with asterisks, the pathways in conformity with the ^{15}N labels are shown in red, and all the systems are with one positive charge.

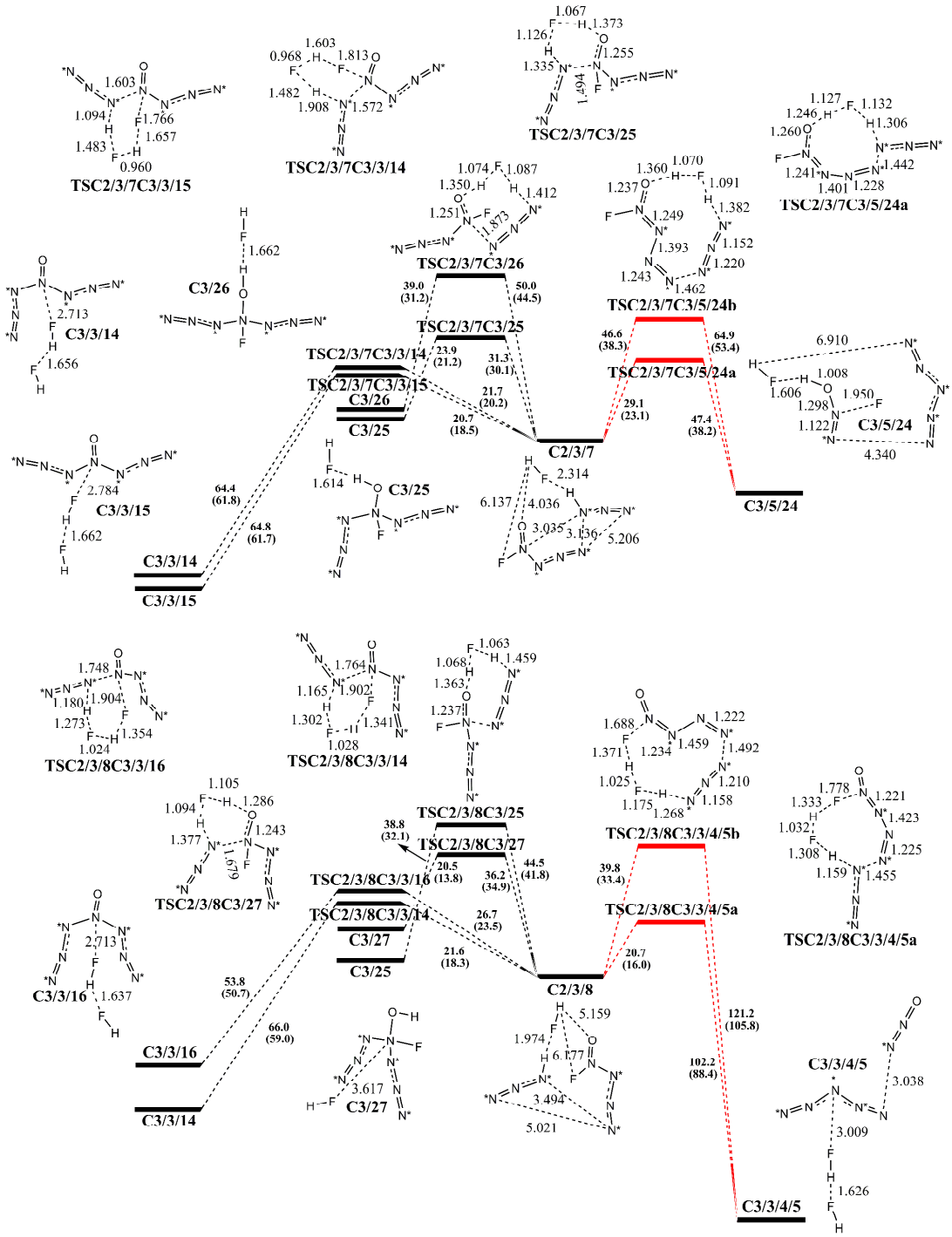

Fig. 10 Schematic potential energy surfaces around N_4OF^+ + HN_3 + HF at the G3B3 level. The activation free energy barriers at 240 K in kcal/mol, (B3LYP/aug-cc-pVDZ values in parentheses), and bond lengths in angstroms. The possible nitrogen atoms labeled by ^{15}N are marked with asterisks, the pathways in conformity with the ^{15}N labels are shown in red, and all the systems are with one positive charge.

G. Formation of N_7O^+ and N_5^+ via N_4OF^+ and HN_3

The reaction pathways between *e*-N_4FO^+ (**7**) or *z*-N_4FO^+ (**8**) and HN_3 (**2**) in the absence of HF (**3**) are presented in Fig. 9. As already mentioned, the barriers involving the proton transfer from **2** to the oxygen of NF_2O^+ in the stepwise mechanisms for the formation of N_4FO^+, are much higher than those involving concerted mechanisms. Consequently, they do not easily lead to the formation of 1-oxo-N_4FO^+ (**10**). The formation of **10** undergoes three transition states and two intermediates (**25** and **28**), and the limiting pathway, the proton transfer to O(N), crosses a barrier of 49.2 kcal/mol. The mechanisms of proton transfer to O(N) is complex. Firstly, **7** or **8** and **2** form complexes **C2/7** or **C2/8** via a long-range Coulombic force with no activation energy barrier. **C2/7** can form **5** along two different pathways via **TSC2/7C5/24a** and **TSC2/7C5/24b**, and crosses barriers of 28.0 and 63.7 kcal/mol, respectively. **24** is highly unstable, and its dissociation barrier is only 3.0 kcal/mol (Fig.

S8). The γ-N of **7** prefers to attach to the α-N of **2** rather than attach to the γ-N of **2**. Another pathway for the formation of **5** starts from **25** through **TS14C4/5a**, and crosses a barrier of 47.5 kcal/mol. Alternatively, **C2/7** can concertedly form **14** and **15** via **TSC2/7C3/14** and **TSC2/7C3/15**, and crosses the barriers of 27.9 and 29.9 kcal/mol, respectively. Consequently in the reaction of **2** with **7**, there is no dominant product formed between **5**, **14** and **15**.

C2/8 can form **5** along three different pathways, via **TSC2/8C3/4/5a**, **TSC2/8C3/4/5b** and **TSC2/8C3/4/5c**, crossing barriers of 24.4, 35.1 and 51.2 kcal/mol, respectively. The γ-N of **8** also prefers to attach to the α-N of **2**, and α-N of **2** is more reactive than γ-N of **2**. It is logical that the reactions involving γ-N of **2** aren't considered for the dissociation of N_7O^+ in the presence of excess HN_3. Alternatively, **C2/8** can form **14** and **16** via **TSC2/8C3/14** and **TSC2/8C3/16**, and crosses barriers of 29.8 and 31.9 kcal/mol, respectively. Consequently, in the reaction of **2** with **8** the dominant product out of **5**, **14** and **16** is probably **5**. Except for the pathway via **TSC2/8C3/4/5b**, all the pathways agree with the observed ^{15}N labels.

HF acts as an auto-catalyst in these reaction systems. Thus, the reactions of **7** or 8 with HN_3 in the presence of HF were investigated and are shown in Fig. 10. Generally, the reaction barriers are lower in the presence of HF than in its absence, however, the presence of HF does not affect the order of the barriers. During the reactions of **7** with **2** in the presence of HF, the formation barriers of **14** and **15** are 21.7 and 20.7 kcal/mol, respectively, while the lower formation barrier of **5** is 29.1 kcal/mol. Consequently, in the reaction of **7** with **2** in the presence of HF the dominant product out of **5**, **14** and **15** is probably **15**. During the reactions of **8** with HN_3 in the presence of HF, the formation barriers of **14** and **16** are 21.6 and 26.7 kcal/mol, respectively, while the lower formation barrier of **5** is 20.7 kcal/mol. Therefore, in the reaction of **8** with HN_3 in the presence of HF the dominant product out of **5**, **13** and **15** is probably **5**.

In conclusion, in the absence of HF, the reaction of *z*-N_4FO^+ **(8)** and HN_3 **(2)** via **TSC2/8C3/4/5a** has the lowest barrier (24.4 kcal/mol), and, in the presence of HF, the production of N_5^+ **(5)** via **TSC2/3/8C3/3/4/5a** has the lowest barrier at the B3LYP level. Although at the G3B3 level the barrier for this reaction is the same (both = 20.7 kcal/mol) as the production of 4-oxo-N_7O^+ **(15)** via **TSC2/3/7C3/3/15**, the consumption of **8** might contribute to the transformation of **7** to **8**. Compared to the barriers of the reactions of NF_2O^+ with HN_3, the reactions of *e*-N_4FO^+ and *z*-N_4FO^+ with HN_3 must cross higher barriers, which may be one of reasons why the subsequent reactions need excess HN_3.

H. Summary of the computational study

In this investigation, the reaction of F_2NO^+ with HN_3 and the subsequent reactions, together with the isomerization and dissociation of N_4FO^+ and N_7O^+, have been studied using B3LYP and G3B3 methods. Whether in the presence or absence of HF, the reaction of F_2NO^+ with HN_3 can produce N_4FO^+ whose primary isomers are *e*-N_4FO^+ (**7**) and *z*-N_4FO^+ (**8**). The decomposition of *e*-N_4FO^+ and *z*-N_4FO^+ to $ONNF^+$ (and subsequently NO^+) crosses a limiting barrier of 21.1 kcal/mol. In accord with the previous study,[4] the self-decomposition barrier of 4-oxo-N_7O^+ via **TS14C4/5a** is 39.5 kcal/mol. Based on the computational results, the formation of N_2O and N_5^+ following the ^{15}N labels can be divided into four cases (Table 2). 1) N_4FO^+ dissociates directly into N_2O and N_2F^+, and then N_5^+ is formed by the reaction of N_2F^+ with HN_3; 2) 4-oxo-N_7O^+ dissociates into N_2O and N_5^+ itself; 3) 4-oxo-N_7O^+ dissociates into N_2O and N_5^+, catalyzed by HN_3; and 4) the reaction between N_4FO^+ and HN_3 produces N_2O and N_5^+. Based on the data in Table 2, the first case has the highest barrier, 38.8 kcal/mol, and is not reasonable. As a matter of fact, its barrier is higher than that of the decomposition to NO^+. In the second case, the barrier, 39.5 kcal/mol, is higher than that of 19.6 kcal/mol of the decomposition to N_2 and 1-oxo-N_5O^+. Therefore, if *syn-syn*-4-oxo-N_7O^+ (**15**) (the lowest energy 4-oxo-N_7O^+ isomer) is formed, it would decompose to NO^+ with evolution of N_2. Consequently, the formation of N_2O and N_5^+ does not imply that 4-oxo-N_7O^+ is the necessary intermediate. In the third case, the barrier of 30.6 kcal/mol is lower than that of 39.5 kcal/mol for the uncatalyzed self-decomposition to N_5^+, but still higher than that of 19.6 kcal/mol for the self-decomposition to NO^+. In the fourth case, *z*-N_4FO^+ and HN_3 produce N_2O and N_5^+ with a barrier of 24.4 kcal/mol in the absence of HF and 20.7 kcal/mol in its presence, while the ^{15}N labels of the products agree with experiment.[4] Based on the analysis of the four cases, 4-oxo-N_7O^+ has not been formed as an intermediate in the reaction of NF_2O^+ with excess HN_3, and N_2O and N_5^+ are probably formed in the 4th case, i.e., by the HF catalyzed reaction of N_4FO^+ with HN_3. The latter reaction involves with **TSC2/3/8C3/3/4/5a** a cyclic transition state containing a 1-oxo-N_7O^+ cation which can decompose to N_5^+ and N_2O with a barrier of only 0.2 kcal/mol and results in the experimentally observed ^{15}N labels.[4] The adjacently longest N-N distance of **TSC2/3/8C3/3/4/5a** is the N of α-position of **2** approaching to N of γ-position of **8**. The distance computed at B3LYP level is 1.455 Å compared with 1.449 Å for experimental[7] (electron diffraction and microwave spectroscopy) N-N single bond length of hydrazine. **TSC2/3/8C3/3/4/5a** involves a 1-oxo-N_7O^+ component as **19**, and it should decompose to N_2O and N_5^+ with few energy barrier. The comparison between geometries of **19** and **TSC2/3/8C3/3/4/5a** is shown in Fig. 11. The solvent effects were also estimated, see Table 2. The result of the 4th case as the optimum pathway is not changed. The correctness of this conclusion was experimentally confirmed by the reaction of unlabeled N_4FO^+ and α- and γ-labeled HN_3 which produced unlabeled N_2O and α- and γ- ^{15}N-labeled N_5^+ (see below).

Table 2 The dissociation pathways following the ^{15}N labels, and their activation free energy barriers at 240 K in kcal/mol and solvent effects[α] for different cases.

Case	Pathway	Barrier		Solvent Effect
		B3LYP	G3B3	
1st	**8→TS8C4/6a**[β]	36.8	38.8	-0.2
2nd	**14→TS14C4/5a**[γ]	36.9	39.5	-3.1
3rd	**C2/14→TSC2/14C5/20**[δ]	25.8	30.6	0.2
4th	**C2/3/8→TSC2/3/8C3/3/4/5a**[ε]	16.0	20.7	-2.9

[α]There are three key parameters, static dielectric constant, dynamic dielectric constant, and solvent radius in this model. The polynomial fitting parameters of static dielectric constant on HF are $a=0.50352\times10^3$, $b=-0.19297\times10^1$ and $c=0.14372\times10^{-2}$. Thus the static dielectric constant

of HF at 240 K was set to 123.17. The dynamic dielectric constant is equal to the square of refraction index. The refraction index of HF at 298 K is 1.1574, and the approximate correction factor of temperature is 0.00045. Thus the dynamic dielectric constant of HF at 240 K was set to 1.280. The solvent radius of HF, recommended by tight calculation of molecular volume using the Monte-Carlo integration, was set to 2.41 angstrom. All the data of chemical and physical properties are taken from ref. 7.

[β]From Fig. 2.

[γ]From Fig. 6.

[δ]From Fig. 7.

[ε]From Fig. 10.

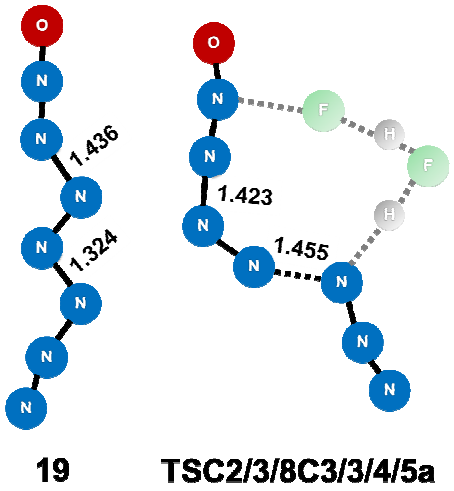

Fig. 11 Computed geometries of **19** and **TSC2/3/8C3/3/4/5a** at B3LYP/aug-cc-pVDZ level. The bond lengths in angstroms and all the systems possess one positive charge.

I. ^{15}N labeling experiment between unlabeled N_4FO^+ and α- and γ-labeled HN_3

In the original report on 4-oxo-N_7O^+, the following ^{15}N labeling experiment was carried out using unlabeled NF_2O^+ and an excess of 50% α- and γ-labeled HN_3, with the ^{15}N label being equally distributed over all five N atoms of N_5^+ and the terminal N of N_2O (Scheme 6).

$$NF_2O^+ + 2\ H\text{-}N^*\text{-}N\text{-}N^* \rightarrow [N^*\text{-}N^*\text{-}N^*\text{-}N^*\text{-}N^*]^+ + N^*\text{-}N\text{-}O + 2\ HF$$

Scheme 6 Distribution of ^{15}N labels in the reaction of unlabeled NF_2O^+ with α- and γ-labeled HN_3.

The formation of a 4-oxo-N_7O^+ cation intermediate was proposed[4] to explain the experimentally observed labels. However, the predicted barrier for the self-decomposition of 4-oxo-N_7O^+ to N_5^+ and N_2O was 42.0 kcal/mol at the B3LYP/6-311G(2df) level of theory. This high barrier was in stark contrast to our inability to experimentally observe 4-oxo-N_7O^+, even at low temperatures, by NMR spectroscopy. Based on the extensive computational study described above, an alternate pathway involving the reaction of N_4FO^+ with HN_3 was proposed yielding the correct ^{15}N distribution while at the same time crossing a barrier of only 20.7 kcal/mol. Furthermore, the predicted cyclic transition state involves a 1-oxo-N_7O^+ component which can decompose with a barrier of only 0.2 kcal/mol to N_5^+ and N_2O. The correctness of the proposed alternate pathway was experimentally tested by the following ^{15}N label experiment between unlabeled N_4FO^+ and 50% α- and γ-labeled HN_3. If 4-oxo-N_7O^+would be the intermediate (Pathways B and C), the products should be N_2O with the terminal N being labeled and N_5^+ with all labels. On the other hand, if the alternate pathway A involving a cyclic 1-oxo-N_7O^+ intermediate is correct, the ^{15}N should be found exclusively in the central and terminal positions of N_5^+ and none in N_2O (Scheme 7).

The results from this labeling experiment are shown in Figure 12. It is clearly seen that only Pathway A agrees with the observed ^{15}N-labels.

The ^{15}N labels are exclusively in the *α*- and *γ*-positions of N_5^+ and none in N_2O. In addition to the labeled N_5^+, strong ^{15}N signals are observed for the protonated form of the *α*- and *γ*-labeled HN_3 starting material, $H_2N_3^+$, due to the well-known[3,13] equilibrium between HN_3 and HF which was used as a solvent for recording the spectra.

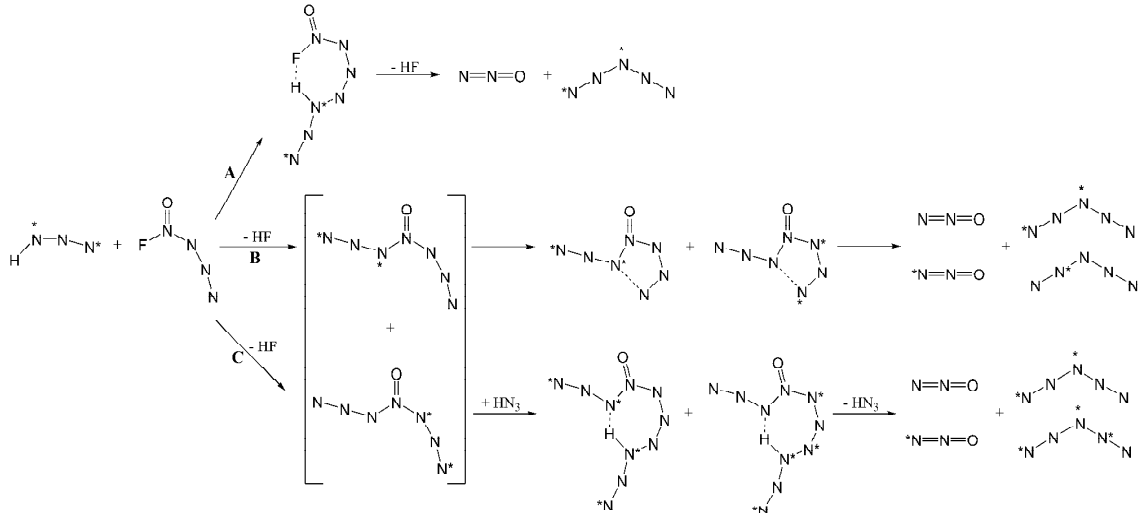

Scheme 7 Distribution of ^{15}N labels (marked by an asterisk) in the reaction of unlabeled N_4FO^+ and 50% α- and γ-labeled HN_3. Pathway A involves a cyclic intermediate containing a 1-oxo-N_7O^+ intermediate and results in unlabeled N_2O and α- and γ-labeled N_5^+, while Pathways B (uncatalyzed) and C (catalyzed by HN_3), involving 4-oxo-N_7O^+ as an intermediate, results in N_2O labeled on the terminal N and N_5^+ labeled in the α-, β- and γ-positions.

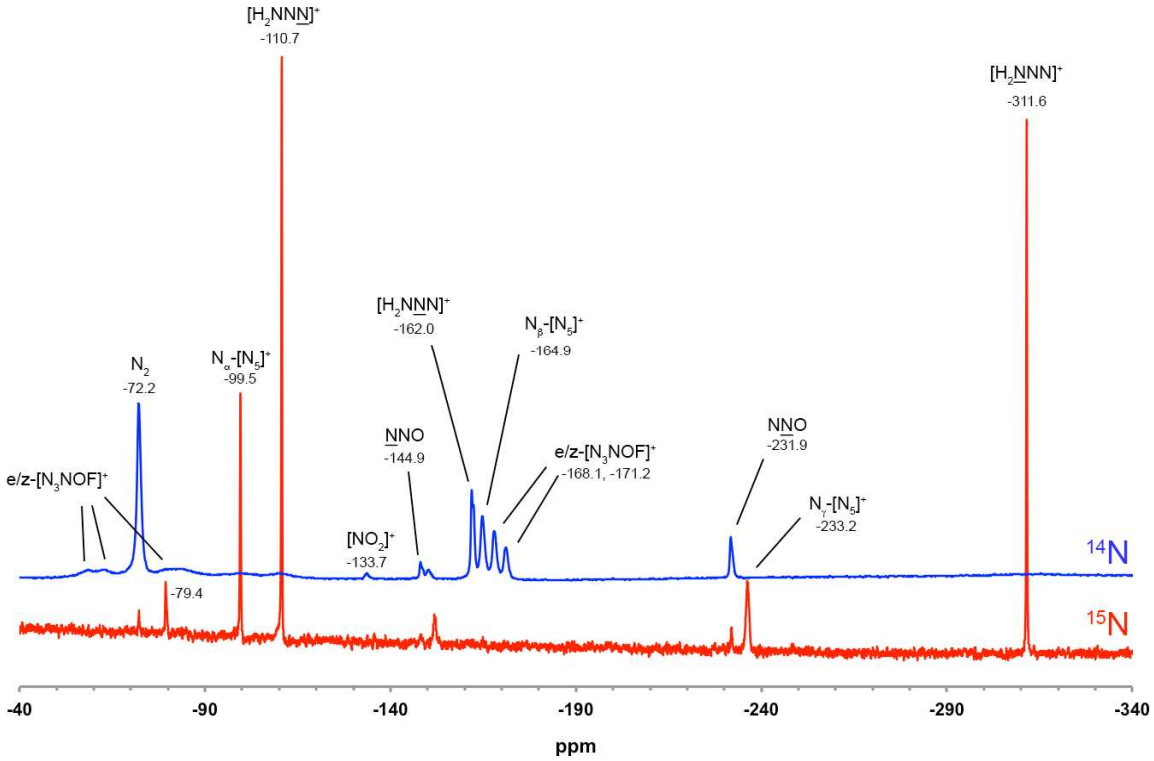

Fig. 12 ^{14}N- and ^{15}N-NMR spectra of the products from the reaction of unlabeled N_4FO^+ and 50% α- and γ-labeled HN_3.

Conclusions

The results from both the computational study and the experimental labeling experiment demonstrate that 4-oxo-N_7O^+ has not been formed in the reaction of NF_2O^+ with excess HN_3. Instead, a competing pathway involving a cyclic transition state **TSC2/3/8C3/3/4/5a,** containing a 1-oxo-N_7O^+ cation which can decompose to N_5^+ and N_2O with a barrier of only 0.2 kcal/mol, produces the observed N_5^+ and N_2O with the correct labels. Although *syn-syn*-4-oxo-N_7O^+ is the minimum energy isomer of N_7O^+ and has reasonably high self-decomposition barriers of 19.6 kcal/mol to NO^+ and N_2, and of 39.5 kcal/mol to N_5^+ and N_2O, it is not formed in the reaction of NF_2O^+ with excess HN_3, and different synthetic approaches must be utilized for its synthesis. The correctness of our conclusions was confirmed by two ^{15}N labeling experiments of unlabeled NF_2O^+ and N_4FO^+ with α- and γ-labeled HN_3 which produced terminally labeled N_2O and N_5^+ with labels in all 5 positions, and unlabeled N_2O and α- and γ-labeled N_5^+, respectively. Our study shows that 1-oxo-N_7O^+ is much less stable than *syn-syn*-4-oxo-N_7O^+, and its instability is responsible for the difficulties to experimentally observe N_7O^+.

Computational methods

The geometry optimization calculations were performed for the reactants, intermediates, transition states and products using DFT (density functional theory) B3LYP method (the exchange-correlation potential is constructed from Becke's three parameter formula for exchange (B3)[14] along with the Lee-Yang-Parr parameter for correlation (LYP)[15]). Then, harmonic frequency analysis calculations were used to verify that each species is a minima or saddle point. To confirm the right connection of each transition state to its forward and backward minima, intrinsic reaction coordinate (IRC)[16,17] calculations were carried out. The refined energies of each species was also calculated at the composite G3B3[18,19] level. For the small molecules and cations, the CCSD(T)[20-24] (the single and double excitation coupled cluster theory including triple excitation non-iteratively) and MP2[25-29] (the second order perturbation theory) methods combined with the frozen-core option, were also used. Dunning's correlation-consistent basis sets[30] aug-cc-pVXZ (X-zeta basis, X=D, T, Q, 5, 6) were used in this study. The moderate basis set aug-cc-pVDZ was combined with B3LYP, and the aug-cc-pVQZ one with MP2 and CCSD(T). The Polarizable Continuum Model[31] (PCM) of integral equation form[32,33] (IEF) was applied to solvent effect calculations on single point energies based on optimized geometries of important pathways at B3LYP/aug-cc-pVDZ level. The calculation of standard enthalpies of formation involved the design of chemical reaction and calculating their enthalpies of reaction. We employed the reaction that the target compound is formed by its constituent atoms in the gas phases. The temperature for computing free energies was 240 K, in accord with the experiment. The free energy activation barriers were derived from the differences between transition states and complexes of reactants or products. All calculations were carried out using the Gaussian 09 program package.[34]

Experimental section

Caution! *Neat HN_3 is highly explosive and should, whenever*

possible, be handled only in solution. N_4FO^+- and N_5^+-salts react violently with water or organic materials. Anhydrous HF can cause severe burns, and skin contact must be avoided.

Materials and Apparatus. All reactions were carried out in Teflon-FEP ampules that were closed by stainless steel valves. Volatile materials were handled in a stainless steel/Teflon-FEP vacuum line.[35] All reaction vessels and the vacuum line were passivated with ClF_3 prior to use. Nonvolatile materials were handled in the dry argon atmosphere of a glove box. The ^{14}N and ^{15}N NMR spectra were recorded at room temperature unlocked in anhydrous HF as solvent on a Bruker AMX-500 NMR instrument using a 5 mm broadband probe. Neat CH_3NO_2 (δ = 0 ppm) was used as an external standard.

The starting materials, $N_4FO^+SbF_6^-$[3] and HN_3[8] were prepared by literature methods. HF was dried by storage over BiF_5.[36]

Reaction of $N_4FO^+SbF_6^-$ with HN_3. In a typical experiment, $N_4FO^+SbF_6^-$ (0.3 mmol) was added to a thin-walled 4 mm o.d. Teflon-FEP ampule, which was closed by a stainless steel valve. On the vacuum line, anhydrous HF (270 mg) was condensed in at -196 °C and the $N_4FO^+SbF_6^-$ was dissolved in the HF at room temperature. The ampule was cooled back to -196 °C, and a mixture of HN_3 (0.4 mmol) and HF (750 mg) was condensed in. The FEP ampule was heat-sealed and slowly warmed to ambient temperature. It was then inserted into a standard 5 mm o.d. glass NMR tube and transferred to the probe of the NMR spectrometer.

Acknowlegements

We acknowledge helpful discussions with Dr. Hai-Bo Chang (Tsinghua University) and Dr. Xiao-Fang Chen (Dalian Institute of Chemical Physics, CAS). The graphical abstract was designed and produced with the help of Mr. Shuo Zhang who graduated from Xi'an Academy of Fine Arts. The work at XAMCRI and FZU was partially supported by the National Science Foundation of China (Nos. 21303133 and 51171046). The work at USC was financially supported by the Office of Naval Research and the Defense Threat Reduction Agency.

Notes and references

1 K. O. Christe, *Prop. Explos. Pyrotech.*, 2007, **32**, 194.
2 K. O. Christe, W. W. Wilson, J. A. Sheehy and J. A. Boatz, *Angew. Chem. Int. Ed.*, 1999, **38**, 2004.
3 W. W. Wilson, R. Haiges, J. A. Boatz and K. O. Christe, *Angew. Chem. Int. Ed.*, 2007, **46**, 3023.
4 K. O. Christe, R. Haiges, W. W. Wilson and J. A. Boatz, *Inorg. Chem.*, 2010, **49**, 1245.
5 A. Vij, X. Zhang and K.O. Christe, *Inorg. Chem.*, 2001, **40**, 416.
6 B. P. Winnewisser, *J. Mol. Spectrosc.*, 1980, **82**, 220.
7 D. R. Lide, *CRC handbook of chemistry and physics*, 84th edition, CRC Press, Boca Raton, FL, 2003-2004.
8 A. Vij, W. W. Wilson, V. Vij, F. S. Tham, J. A. Sheehy and K. O. Christe, *J. Am. Chem. Soc.*, 2001, **123**, 6308.
9 P. Botschwina, P. Sebald, M. Bogey, C. Demuynck and J.-L. Destombes, *J. Mol. Spectrosc.*, 1992, **153**, 255.
10 D. A. Dixon, D. Feller, K. O. Christe, W. W. Wilson, A. Vij, V. Vij, H. D. B. Jenkins, R. M. Olson, and M. S. Gordon, *J. Am. Chem. Soc.*, 2004, **126**, 834.
11 T. Yu, H.-B. Chang, W.-P. Lai and X.-F. Chen, *Polym. Chem.*, 2011, **2**, 89230.
12 W.-G. Xu, G.-L. Li, L.-J. Wang, S. Li and Q.-S. Li, *Chem. Phys. Lett.*, 1999, **314**, 300.
13 K. O. Christe, W. W. Wilson, D. A. Dixon, S. I. Khan, R. Bau, T. Metzenthin and R. Lu, *J. Am. Chem. Soc.,* 1993, **115**, 1836.
14 A. D. Becke, *J. Chem. Phys*, 1993, **98**, 5648.
15 C. Lee, W. Yang, and R. G. Parr, *Phys. Rev. B*, 1988, **37**, 785.
16 C. Gonzalez and H. B. Schlegel, *J. Chem. Phys,*, 1989, **90**, 2154.
17 C. Gonzalez and H. B. Schlegel, *J. Chem. Phys,*, 1991, **95**, 5853.
18 A. G. Baboul, L. A. Curtiss, P. C. Redfern and K. Raghavachari, *J. Chem. Phys.*, 1999, **110**, 7650.
19 L. A. Curtiss, K. Raghavachari, P. C. Redfern, V. Rassolov and J. A. Pople, *J. Chem. Phys.*, 1998, **109**, 7764.
20 J. Cizek, *Adv. Chem. Phys.*, 1969, **14**, 35.
21 G. D. Purvis III and R. J. Bartlett, *J. Chem. Phys.*, 1982, **76**, 1910.
22 G. E. Scuseria, C. L. Janssen and H. F. Schaefer III, *J. Chem. Phys.*, 1988, **89**, 7382.
23 G. E. Scuseria and H. F. Schaefer III, *J. Chem. Phys.*, 1989, **90**, 3700.
24 J. A. Pople, M. Head-Gordon, and K. Raghavachari, *J. Chem. Phys*, 1987, **87**, 5968.
25 M. Head-Gordon, J. A. Pople and M. J. Frisch, *Chem. Phys. Lett.*, 1988, **153**, 503.
26 S. Saebø and J. Almlöf, *Chem. Phys. Lett.*, 1989, **154**, 83.
27 M. J. Frisch, M. Head-Gordon and J. A. Pople, *Chem. Phys. Lett.*, 1990, **166**, 275.
28 M. J. Frisch, M. Head-Gordon and J. A. Pople, *Chem. Phys. Lett.*, 1990, **166**, 281.
29 M. Head-Gordon and T. Head-Gordon, *Chem. Phys. Lett.*, 1994, **220**, 122.
30 T. H. Dunning Jr., *J. Chem. Phys.*, 1989, **90**,1007.
31 J. Tomasi, B. Mennucci, and R. Cammi, *Chem. Rev.*, 2005, **105**, 2999.
32 J. Tomasi, B. Mennucci, and E. Cancès, *J. Mol. Struct. (Theochem)*, 1999, **464**, 211.
33 G. Scalmani and M. J. Frisch, *J. Chem. Phys*, 2010, **132**, 114110.
34 *Gaussian 09*, Revision B. 01, AM. J. Frisch, G. W. Trucks, H. B. Schlegel, G. E. Scuseria, M. A. Robb, J. R. Cheeseman, G. Scalmani, V. Barone, B. Mennucci, G. A. Petersson, H. Nakatsuji, M. Caricato, X. Li, H. P. Hratchian, A. F. Izmaylov, J. Bloino, G. Zheng, J. L. Sonnenberg, M. Hada, M. Ehara, K. Toyota, R. Fukuda, J. Hasegawa, M. Ishida, T. Nakajima, Y. Honda, O. Kitao, H. Nakai, T. Vreven, J. A. Montgomery, Jr., J. E. Peralta, F. Ogliaro, M. Bearpark, J. J. Heyd, E. Brothers, K. N. Kudin, V. N. Staroverov, R. Kobayashi, J. Normand, K. Raghavachari, A. Rendell, J. C. Burant, S. S. Iyengar, J. Tomasi, M. Cossi, N. Rega, J. M. Millam, M. Klene, J. E. Knox, J. B. Cross, V. Bakken, C. Adamo, J. Jaramillo, R. Gomperts, R. E. Stratmann, O. Yazyev, A. J. Austin, R. Cammi, C. Pomelli, J. W. Ochterski, R. L. Martin, K. Morokuma, V. G. Zakrzewski, G. A. Voth, P. Salvador, J. J. Dannenberg, S. Dapprich, A. D. Daniels, O. Farkas, J. B. Foresman, J. V. Ortiz, J. Cioslowski and D. J. Fox, Gaussian, Inc., Wallingford CT, 2009.
35 K. O. Christe, W. W. Wilson, C. J. Schack and R. D. Wilson, *Inorg. Synth.*, 1986, **24,** 39.
36 K. O. Christe, W. W. Wilson and C. J. Schack, *J. Fluorine. Chem.*, 1978, **11,** 71.

[a]*Computer-Aided Energetic Materials Design Group, Xi'an Modern Chemistry Research Institute, Xi'an 710065, P. R. China.*
[b]*Loker Research Institute, University of Southern California, Los Angeles, CA 90089-1661, USA*
[c]*Multiscale Computational Materials Facility, School of Materials Science and Engineering, Fuzhou University, Fuzhou 350108, P. R. China.*
**Corresponding authors: Tel: (+86) 029-88294020, E-mail: fischer@wo.com.cn (T. Yu); Tel: (+1) 213-7403552, E-mail: kchriste@usc.edu (K. Christe); Tel: (+86) 0591-38725008, E-mail: wubo@fzu.edu.cn (B. Wu).*

† Electronic supplementary information (ESI) available: optimized structures of **1** to **6** at the B3LYP/6-311++G** level, the computed enthalpies of formation in gas phase at 298.15 K for **1** to **6** at the B3LYP/6-311++G** and CBS-QB3 levels, compounds and cations mapping list for their serial numbers and supplementary reaction pathways.

Graphical Abstract Results from a combined computational and experimental study show that 1-oxo-N_7O^+ (right) is much less stable than 4-oxo-N_7O^+ (left), and that its facile decomposition to N_5^+ and N_2O impedes the synthesis of 4-oxo-N_7O^+ from NF_2O^+ or N_3NFO^+ and excess HN_3.